



# An analytical model of rumpling in thermal barrier coatings

D.S. Balint\*, J.W. Hutchinson

*Division of Engineering and Applied Sciences, Harvard University, Cambridge, MA 02138, USA*

Received 6 May 2004; accepted 4 November 2004

---

## Abstract

Multilayer thermal barrier coatings (TBCs) deposited on superalloy turbine blades provide protection from combustion temperatures in excess of 1500 °C. One of the dominant failure modes comprises cracking from undulation growth, or rumpling, of the highly compressed oxide layer that grows between the ceramic top coat and the intermetallic bond coat. In this paper, a mechanistic model providing an analytical approximation of undulation growth is presented for realistic cyclic thermal histories. Thickening, lateral growth straining and high temperature yielding of the oxide layer are taken into account. Undulation growth in TBC systems is highly nonlinear and characterized by more than 20 material and geometric parameters, highlighting the importance of a robust yet computationally efficient model. At temperatures above 600 °C, the bond coat creeps. Thermal expansion mismatch occurs between the superalloy substrate and the oxide layer and, in some systems, the bond coat. In addition, some bond coats, such as PtNiAl, exhibit a martensitic phase transformation accompanied by nearly a 1% linear expansion, giving rise to a large effective mismatch. These two mismatches promote undulation growth. Nonlinear interaction between the stress in the bond coat induced by the constraining effect of the thick substrate and normal tractions applied at the surface of the bond coat by the compressed, undulating oxide layer produces an increment of undulation growth during each thermal cycle, before the stress decays by creep. A series of problems for systems without the ceramic top coat are used to elucidate the mechanics of undulation growth and to replicate trends observed in a series of experiments and in prior finite-element simulations. The model is employed to study for the first time the effect on

---

\*Corresponding author. Engineering Department, Cambridge University, Trumpington Street, Cambridge CB2 1PZ, UK. Tel.: +44 1223 339883; fax: +44 1223 332662.

*E-mail address:* [dsb38@cam.ac.uk](mailto:dsb38@cam.ac.uk) (D.S. Balint).

undulation growth of a shift in the temperature range over which the transformation occurs, as well as the relative importance of the transformation compared to thermal expansion mismatch. The role of the top coat and other viable ways of reducing undulation growth are considered.

© 2004 Elsevier Ltd. All rights reserved.

*Keywords:* Thermomechanical processes; Creep; Phase transformation; Layered material; Analytical modeling

---

## 1. Introduction

Oxide coatings with low thermal conductivity are used to protect internally cooled components from the extreme temperatures of their surroundings. This is achieved by establishing a thermal gradient across the coating that lowers the temperature of the underlying substrate (usually an alloy), often by several hundred degrees. The most important application is on hot section components in turbine engines used for aircraft propulsion and power generation (Evans et al., 2001b). The maximum material temperatures attained in these systems often exceed 1300 °C.

A full thermal barrier system consists of four layers (Evans et al., 2001b). The thermally insulating outer layer, or top coat, is an oxide, typically 100 μm of yttria-stabilized zirconia (YSZ). It is deposited onto an intermetallic layer called the bond coat that is roughly 50 μm thick. In addition to helping the thermal barrier adhere to the substrate, the bond coat is the source of the Al that allows formation of a protective layer of alumina, referred to as the thermally grown oxide (TGO). During service, the TGO grows to be 5 μm thick or more. The bond coat and the top coat creep at temperatures in excess of 600 °C. Both layers are modeled at elevated temperatures as power-law creeping materials. The TGO can be modeled as elastic/perfectly plastic at 1150 °C and elastic at all other temperatures (Karlsson et al., 2002). In addition, the alumina experiences in-plane lateral growth as well as thickening. Lateral growth produces the compressive strain in the alumina driving the undulation growth (Karlsson et al., 2002; Clarke, 2003). Undulations that develop in the TGO layer (cf. Fig. 1), otherwise known as rumpling or ratcheting, and the stresses they induce in the YSZ outer layer may be responsible for cracks that limit the lifetime of the coating (Evans et al., 2001a; Mumm et al., 2001; Xu et al., 2003; Chen et al., 2003a).

Various attempts have been made to simulate the shape deformations, the stresses and the crack extension by using finite-element methods (Karlsson and Evans, 2001; Karlsson et al., 2002; Xu et al., 2003). The results have provided some appreciation for trends in undulation growth with the properties of the bond coat, the TGO and the YSZ top coat. They have also elucidated the crucial roles of the lateral growth in the TGO and of its plastic response at elevated temperature (Karlsson et al., 2002). The finite-element models are limited in two primary ways: (i) time varying properties such as creep cannot be readily addressed, because of the computational

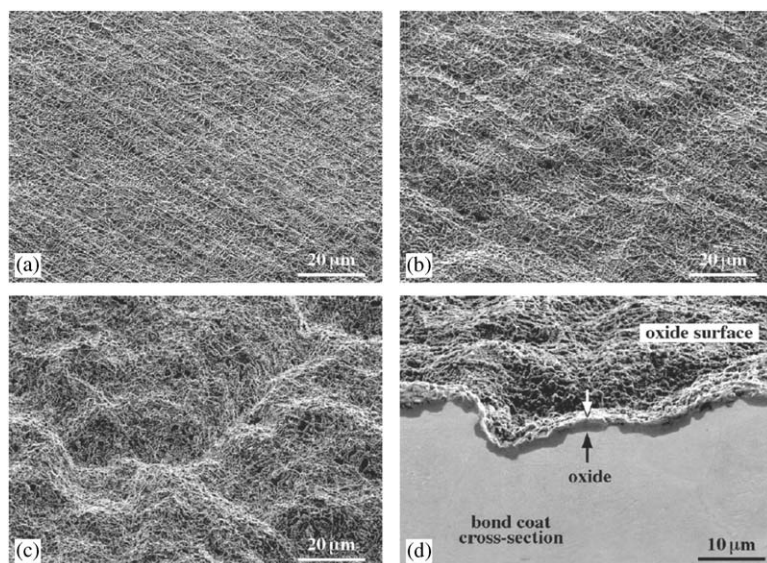


Fig. 1. A specimen without a protective outer layer tested by Tolpygo and Clarke (2000) for a cyclic thermal history with a peak temperature of 1200 °C that shows oxide rumpling on a PtNiAl bond coat after (a) 1 cycle, (b) 10 cycles and (c) 50 cycles.

expense; the prior assessments treat the bond coat and YSZ as elastic/perfectly plastic; (ii) the number of material and length parameters characterizing the systems is large, limiting the realizable scope of sensitivity studies. These deficiencies place a high priority on the development of a computationally efficient model.

In this paper, an analytical model of undulation growth is presented in a complete four-layer system for cyclic thermal histories. Many of the important features of the system are incorporated. Results for systems with and without the top coat layer will be presented, but most of the results will be for systems without top coats. TBCs without a topcoat are also widely employed in turbine systems, and, moreover, they constitute an important body of experiments carried out to elucidate rumpling behavior (Tolpygo and Clarke, 2000, 2004a, b).

The model is used to explore several effects. Initially, all of the known properties of a system with a PtNiAl bond coat (Pan et al., 2003) are used to examine trends: including bond coat creep, the martensite transformation and the role of the top coat in rumpling. Thereafter, a sensitivity study is conducted to compare the predictions of the model with experiments, and to connect with finite-element models that use time invariant plasticity (Karlsson and Evans, 2001; Karlsson et al., 2002; Xu et al., 2003). A first study on the dependence of undulation growth on the temperatures specifying the martensite transformation is presented. Simulations are also performed revealing the effect of the top coat on undulation growth and the associated stresses driving top coat cracking.

2. Material descriptions

The list of parameters in a full model of rumpling is extensive (over 20), making it difficult to establish connections between properties and specific phenomena. A model is derived that makes use of an analytical approximation for the creep of the bond coat and YSZ and its interaction with the TGO. The equations governing the model take the form of a set of coupled, ordinary nonlinear differential equations that can be readily solved numerically. Although the formulation is general with respect to material properties, the focus is on systems with PtNiAl bond coats. The model is built upon the framework developed by Balint and Hutchinson (2003). Details from this earlier work are repeated only where necessary.

The system depicted in Fig. 2 consists of a thin, isotropic elastic/perfectly plastic TGO film with Young’s modulus  $E^{(3)}$ , Poisson’s ratio  $\nu^{(3)}$ , coefficient of thermal expansion,  $\alpha^{(3)}$ , thickness,  $h^{(3)}$ , and high temperature yield stress,  $\sigma_R^{(3)}$  (established by the experimentally measured growth stress). At the beginning of thermal cycling (at time  $t = 0$ ), the TGO is assumed to have an initial sinusoidal undulation with amplitude,  $\delta_0$ , and half-wavelength,  $L$ . Beneath the TGO is the bond coat layer of thickness,  $h^{(2)}$ , with isotropic elastic properties given by  $E^{(2)}$ ,  $\nu^{(2)}$ , and  $\alpha^{(2)}$ , and

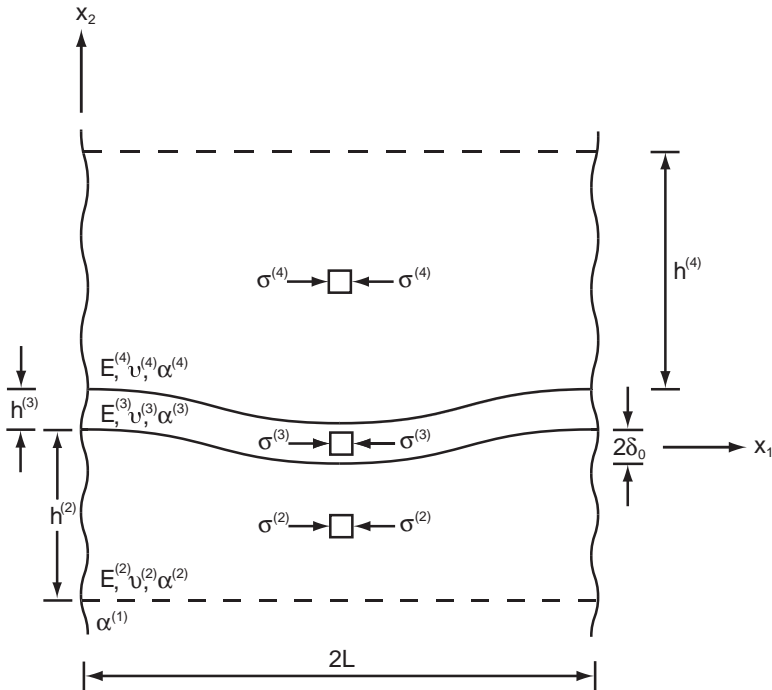


Fig. 2. A schematic of a four-layer thermal barrier system with an undulation in the oxide layer. The metallic bond coat and protective outer layer are modeled as though they are infinite in the  $x_2$ -direction. The dashed lines indicate the actual boundaries.

inelastic behavior characterized by power-law creep with reference creep-rate,  $\dot{\epsilon}_R^{(2)}$ , and reference stress,  $\sigma_R^{(2)}$ . Above the TGO is the YSZ layer. With a dot over a symbol denoting its time rate of change, the total strain rate for the bond coat is given by:

$$\begin{aligned} \dot{\epsilon}_{ij}^{(2)} = & \frac{1 + \nu^{(2)}}{E^{(2)}} \dot{\sigma}_{ij}^{(2)} - \frac{\nu^{(2)}}{E^{(2)}} \dot{\sigma}_{kk}^{(2)} \delta_{ij} \\ & + \alpha^{(2)} \dot{T} \delta_{ij} + \frac{3}{2} \dot{\epsilon}_R^{(2)} \left( \frac{\sigma_e^{(2)}}{\sigma_R^{(2)}} \right)^{n^{(2)}-1} \frac{s_{ij}^{(2)}}{\sigma_R^{(2)}} e^{-T_R^{(2)}/T}, \end{aligned} \quad (1)$$

where  $s_{ij}^{(2)}$  is the deviatoric stress and the effective stress is given by

$$\sigma_e^{(2)} = \sqrt{\frac{3}{2} s_{kl}^{(2)} s_{kl}^{(2)}}. \quad (2)$$

Here,  $T$  is the temperature and  $T_R^{(2)}$  (both in K) defines the temperature dependence of the creep strength. The YSZ top coat is highly anisotropic, both elastically and inelastically. Anisotropic constitutive models for characterizing their creep behavior are being developed. In the meantime, Eq. (1) (with quantities designated by a superscript 4) will be used to characterize the in-plane behavior of YSZ relevant to the present model.

Recent experimental results have shown that platinum-modified nickel aluminide bond coats (PtNiAl) undergo a martensitic phase transformation in the vicinity of 600–700 °C accompanied by nearly a 1% linear expansion during heat-up (Chen et al., 2003b). Independently of the transformation, the material exhibits power-law creep with creep strength that decreases rapidly as the temperature increases (cf. Eq. (1)). Material constants that are valid for all temperatures are given in the literature for as-fabricated and thermally cycled bond coats (Pan et al., 2003). Calculations presented in this paper use, in Eq. (1),  $\dot{\epsilon}_R^{(2)} = 0.2 \text{ s}^{-1}$ ,  $T_R^{(2)} = 15 \times 10^3 \text{ K}$ ,  $\sigma_R^{(2)} = 25 \text{ MPa}$ , which is the yield stress of PtNiAl at 1150 °C, and  $n^{(2)} = 4$ , all consistent with the experimental findings. The reference temperature  $T_R^{(2)}$  is a fitting parameter from (Pan et al., 2003) that does not have a particular physical significance. The elastic properties are  $E^{(2)} = 115 \text{ MPa}$ ,  $\nu^{(2)} = 0.27$ , and  $\alpha^{(2)} = 16 \times 10^{-6} \text{ }^\circ\text{C}^{-1}$ . The volume change accompanying the phase transformation is modeled using an effective thermal expansion coefficient of  $86 \times 10^{-6} \text{ }^\circ\text{C}^{-1}$  for the bond coat between 600 and 700 °C on the heat-up, and between 550 and 450 °C on the cool-down, giving 0.7% linear strain change relative to the substrate occurring over a span of 100 °C (Chen et al., 2003b).

Detailed creep data for the TGO are not presently available. However, stress measurements indicate that under high temperature conditions these materials deform at an essentially constant stress, the growth stress. In prior models, equating this stress to the yield strength at the peak temperature has satisfactorily accounted for the shape deformations of the TGO and the ensuing stress distribution. Its elastic properties are  $E^{(3)} = 375 \text{ GPa}$ ,  $\nu^{(3)} = 0.2$  and  $\alpha^{(3)} = 8.5 \times 10^{-6} \text{ }^\circ\text{C}^{-1}$ . Below 1150 °C, the oxide is taken to be elastic, because minimal accumulation of creep strain occurs during cool-down and heat-up. Under most circumstances, in the model, yield in the TGO occurs for a portion of every cycle at 1150 °C.

An associated effect is that the oxide layer loses incremental bending stiffness once it has yielded, such that the moment carried by the layer relaxes to zero as further lateral growth occurs. This has a profound effect on undulation growth. Effectively, the moment is bounded by the limit moment associated with the yield stress at the peak temperature and it relaxes when the TGO is at yield due to lateral growth. If the oxide did not yield, the elastic bending moment induced in the layer would increase as the amplitude of the undulation grows and would eventually become large enough to shut off further undulation growth. At the end of the isothermal part of the cycle, cooling begins and the oxide responds elastically recovering its incremental stiffness.

It is now established that lateral growth straining accompanies thickening of the TGO at elevated temperatures due to the formation of new oxide on internal grain boundaries. This strain produces in-plane compressive stress.<sup>1</sup> A normal growth strain is also part of the oxidation process. Simulations show that the thickness of the oxide has a strong influence on undulation growth because of its effect on the net in-plane force of the oxide layer and on its bending stiffness. However, the misfit between the oxide and the layers adjacent to it that results from the normal growth strain is relatively small and is neglected.

At the peak temperature, the oxide layer thickens parabolically with time, i.e.

$$\dot{h}^{(3)} = \frac{k_p}{2h^{(3)}}, \quad (3)$$

where the constant  $k_p$  has dimensions  $\text{m}^2 \text{s}^{-1}$  and is chosen such that the oxide thickens from 0.5 to 3  $\mu\text{m}$  in 100 h at 1150 °C. Based on prior assessments, the correlation between the lateral growth strain rate and the rate of thickening is taken as (Evans et al., 2001a; Clarke, 2003):

$$\dot{\epsilon}_G = \frac{\dot{h}^{(3)}}{d}, \quad (4)$$

where the constant  $d$  is chosen such that 5% lateral growth strain occurs over 100 h at 1150 °C. Neither thickening nor lateral growth straining is assumed to occur below 1150 °C.

### 3. Layer stresses

#### 3.1. Substrate

In the model, the top coat is bonded to an infinitely thick, elastically isotropic substrate representing the superalloy (cf. Fig. 2) with  $\alpha^{(1)} = 14 \times 10^{-6} \text{ } ^\circ\text{C}^{-1}$ . The modulus of the substrate does not play a part in the model because any expansion or contraction of the thick substrate due to changes in temperature is imposed on the layers above it.

<sup>1</sup>Fluctuations in the oxide stress with changes in temperature are primarily the result of thermal mismatch with the substrate.

### 3.2. Bond coat

The system depicted in Fig. 2 is subjected to a cyclic thermal history that begins at 1150 °C, representing the surface temperature in a turbine engine. The state of the system at  $t = 0$  is taken to approximate that of an as-deposited thermal barrier coating system. It is assumed that a thin TGO (0.5  $\mu\text{m}$ ) has grown during deposition, and an in-plane compressive stress equal in magnitude to the yield stress has developed as a result of lateral growth. The bond coat is assumed to be stress-free. In all the simulations carried out here, the temperature is assumed to be uniform throughout the layered system, although temperature differences from layer to layer could be taken into account. First, the system is cooled steadily to room temperature, 25 °C. Because the hold-time at room temperature is inconsequential, heat-up of the system begins as soon as room temperature is attained. The temperature is brought up to its peak value, 1150 °C, and is subsequently held. The cycle is then repeated. Most simulations were performed with a 1-min cool-down, a 1-min heat-up, and a 1-h hold at 1150 °C. The model can be used to explore other cyclic thermal histories, including the effect of other peak temperatures, but this particular cycle has been widely used in laboratory experiments on TBC systems.

The complete state of stress in the bond coat consists of a superposition of the stresses resulting from the sinusoidal normal traction applied at the surface of the bond coat by the compressed, undulating TGO film,  $p^{(2)} \sin(\pi x_1/L)$ , and the equi-biaxial stress  $\sigma^{(2)}$  (the two axes being  $x_1$  and  $x_3$ ; cf. Fig. 3).<sup>2</sup> The stress field resulting from a sinusoidal normal traction applied at the surface of an elastic half-space differs only slightly from what is predicted for steady-state pure power-law creep under the same loading (Balint and Hutchinson, 2003). As a result, elasticity in the bond coat has little direct influence on undulation growth at elevated temperatures and can be neglected. However, elastic strains in Eq. (1) are essential to creep relaxation of the equi-biaxial stress. To determine the history of the equi-biaxial stress, the undulation and the component of stress normal to the layer are ignored, consistent with the assumptions on undulations with small slopes detailed in the next section. The substrate imposes its strain on the bond coat such that

$$\dot{\alpha}^{(2)} = \frac{E^{(2)}}{1 - \nu^{(2)}} \left[ -\frac{\dot{\epsilon}_0^{(2)}}{2} \left( \frac{\sigma^{(2)}}{\sigma_0^{(2)}} \right)^{n^{(2)}} e^{-T_R^{(2)}/T} + \text{sign}(\sigma_{11}^{(2)}) (\alpha^{(1)} - \alpha^{(2)}) \dot{T} \right]. \quad (5)$$

In Eq. (5), the equi-biaxial stress is decomposed into its magnitude,  $\sigma^{(2)} \equiv |\sigma_{11}^{(2)}| = |\sigma_{33}^{(2)}|$ , and its sign,  $\text{sign}(\sigma_{11}^{(2)})$ . At the peak temperature,  $\dot{T} = 0$  and stress relaxation occurs by creep. The equation for the equi-biaxial stress rate in the top coat has the same form as Eq. (5) with due regard for the material parameters.

Simple numerical integration of Eq. (5) gives the cyclic history of the equi-biaxial stress in the PtNiAl bond coat, plotted against temperature in Fig. 4. The difference between the effective thermal strain in the bond coat (as it would be if not for the constraint imposed by the thick substrate) and the thermal strain in the substrate,

<sup>2</sup>The model can be easily adapted for any biaxial stress state.

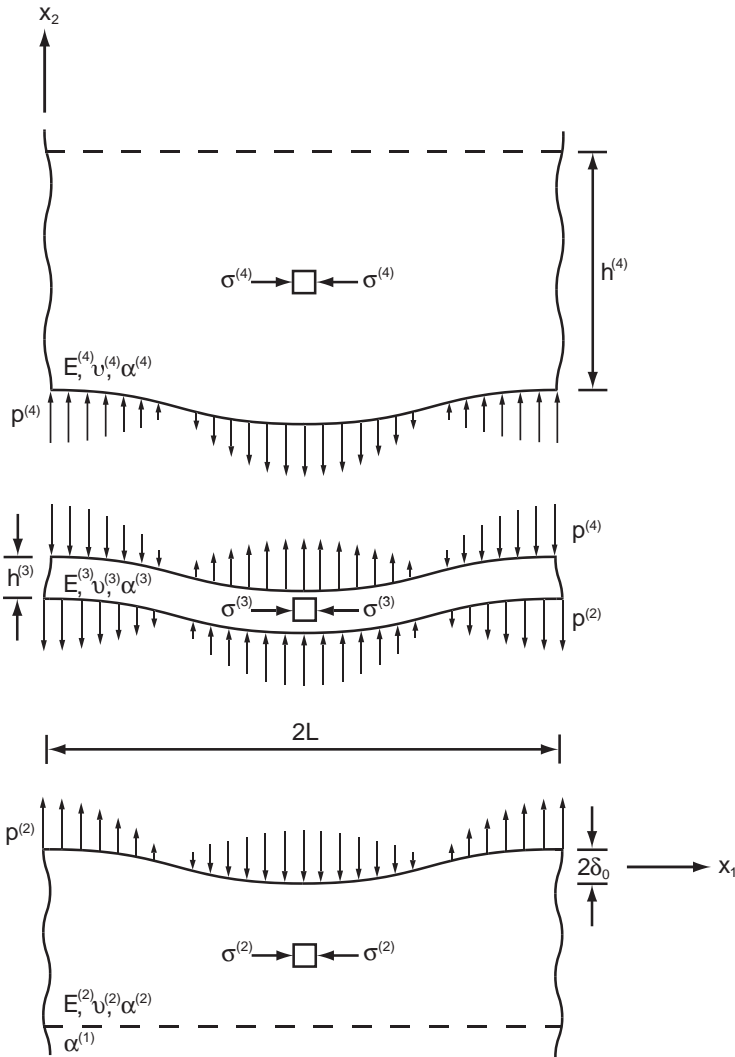


Fig. 3. The system is modeled by first decoupling the layers. Here, the sinusoidal interface tractions that result from the in-plane compressive stress in the undulating oxide layer are shown. The equations written for each layer are then re-coupled to give a complete description of undulation growth.

shown in Fig. 5 as a function of temperature, is helpful in understanding the effect of the reversible, martensitic phase transformation. Each numbered point in these two figures corresponds to the same characteristic point in a thermal cycle. The thermal history begins at point 1 with the system at 1150 °C and with a stress-free bond coat. Point 1 corresponds to the end of the isothermal period, at 1150 °C, for subsequent thermal cycles. (There is virtually no difference in the stress between the first and

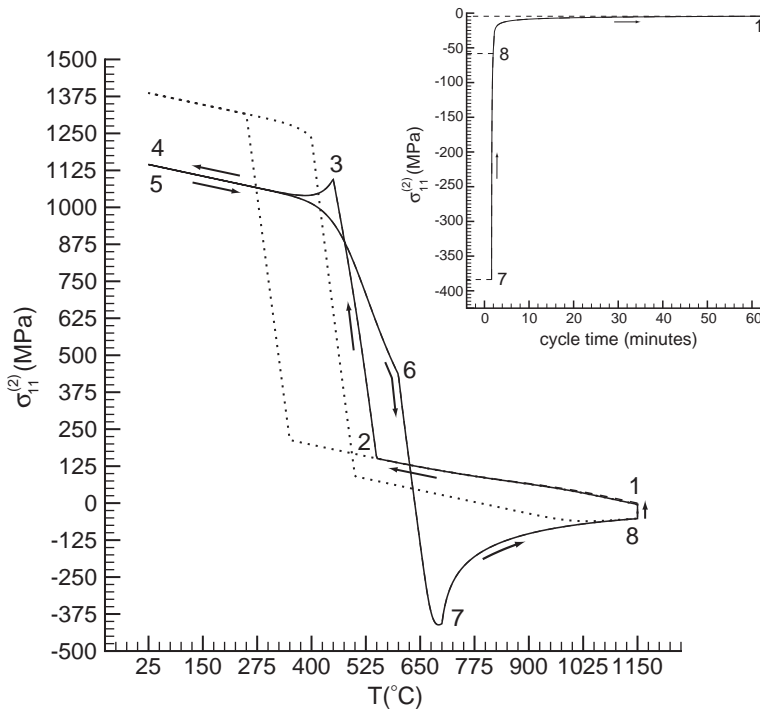


Fig. 4. The equi-biaxial stress cycle in a PtNiAl bond coat when subjected to the thermal history described in Section 3. Most of the total undulation growth per cycle occurs between points 7 and 1, when the creep strength is low and the stress is large (cf. inset). The dotted line shows the stress cycle for a modified phase transformation; the hysteresis in Fig. 5 is shifted by  $-200\text{ }^{\circ}\text{C}$  (cf. Section 5).

subsequent cycles.) Creep is unimportant between points 1 and 2 when the stress is small and the creep strength is increasing. The stress increase during this interval is nearly linear, and is primarily a result of thermal strain mismatch with the substrate. The reverse phase transformation, accompanied by a volumetric contraction, begins at point 2 ( $550\text{ }^{\circ}\text{C}$ ) and ends at point 3 ( $450\text{ }^{\circ}\text{C}$ ). The creep strength is much greater at intermediate temperatures than at the peak temperature. In addition, the strain rate during the phase transformation is very large. Together, these give a nearly linear elastic response for the equi-biaxial stress in the bond coat between points 2 and 3 with only minimal relaxation. Creep relaxation is significant only at the beginning of the interval marked by points 3 and 4 ( $25\text{ }^{\circ}\text{C}$ ); as the temperature decreases further, the creep strength quickly becomes sufficiently large to preclude further stress relaxation. From point 5 ( $25\text{ }^{\circ}\text{C}$ ) to point 6 ( $600\text{ }^{\circ}\text{C}$ ), the stress begins to decrease elastically as a result of thermal strain mismatch with the substrate, but as the temperature is elevated, creep relaxation becomes important. The phase transformation begins at point 6, with the bond coat expanding relative to the substrate leading to a stress of about  $-425\text{ MPa}$  at the end of the transformation at point 7 ( $700\text{ }^{\circ}\text{C}$ ). The bond coat becomes increasingly susceptible to undulation growth from point 7

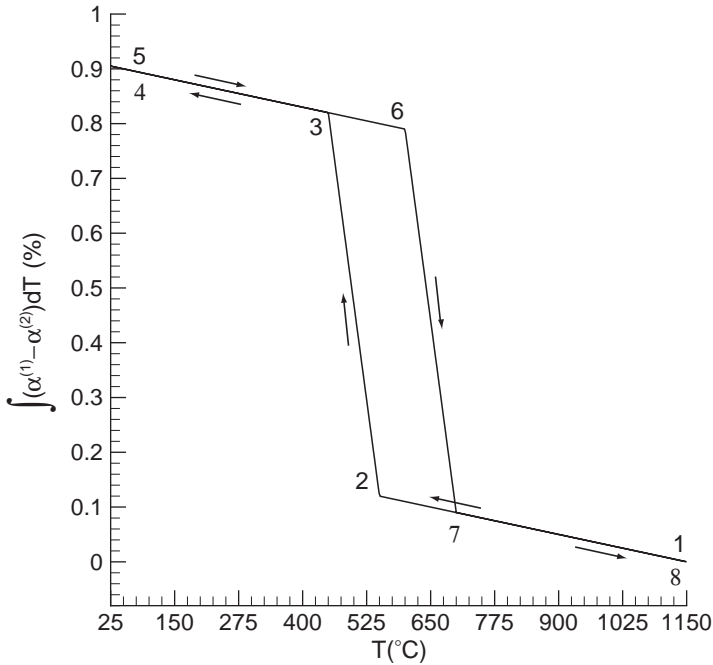


Fig. 5. Thermal strain mismatch between the PtNiAl bond coat and the substrate when subjected to a thermal cycle as described in Section 3. In the simulations presented in this paper, the bond coat is strain-free at 1150 °C, as indicated here.

until the peak temperature is reached at point 8 (1150 °C). The equi-biaxial stress is only –60 MPa at the start of the isothermal period, but, nevertheless, this stress can still be significant since the bond coat has extremely low creep strength at 1150 °C. So low, in fact, that a PtNiAl bar subjected to a uniaxial tensile stress of 50 MPa would undergo straining at a rate of approximately 1% per second. The portion of the thermal cycle where the PtNiAl bond coat is most susceptible to undulation growth is the period beginning with the end of the phase transformation on the heat-up (point 7) and ending at the completion of the isothermal period (point 1).

The effect on the equi-biaxial stress of a shift of the phase transformation hysteresis loop by –200 °C is also shown in Fig. 4. The most important effect, whose consequence is investigated in detail in Section 5, is a significant lowering of the stress at higher temperatures that increases the resistance of the bond coat to deformation by creep. Shifting the transformation loop to lower temperatures confines the largest stresses to lower temperatures where the deformations are elastic and reversible.

### 3.3. Oxide layer

Sinusoidal initial undulations are assumed such that the departure of the mid-plane of the oxide layer from planarity at  $t = 0$  is prescribed by the

normal displacement

$$w_0(x_1) = \delta_0 \cos(\pi x_1/L). \quad (6)$$

As an approximation, the sinusoidal shape is preserved such that the *additional* normal displacement of the undulation at later times is

$$w(x_1, t) = \delta(t) \cos(\pi x_1/L). \quad (7)$$

The half-wavelength of the undulation,  $L$ , is fixed. If no other changes occurred, the in-plane compressive stress in the oxide layer would decrease as the undulation amplitude grows due to the resultant increase in overall length of the layer relative to that in the planar state. Lateral growth at the peak temperature and stress changes due to thermal mismatch with the substrate also contribute to the equation for the magnitude of the overall elastic stress rate in the oxide:

$$\dot{\sigma}^{(3)} = \text{sign}(\sigma_{11}^{(3)}) \left[ \bar{E}^{(3)} \left( \frac{\pi^2(\delta_0 + \delta)\dot{\delta}}{L^2} - \dot{\epsilon}_G \right) + \frac{E^{(3)}}{1 - \nu^{(3)}} (\alpha^{(1)} - \alpha^{(3)}) \dot{T} \right], \quad (8)$$

with  $\sigma^{(3)} = |\sigma_{11}^{(3)}|$  and  $\bar{E}^{(3)} = E^{(3)}/(1 - \nu^{(3)^2})$ . This equation is used except when yielding occurs at 1150 °C due to the lateral growth strain. When yielding occurs, the stress in the oxide is maintained at the yield stress until cool-down starts or unloading occurs. A more sophisticated creep representation of oxide plasticity would probably do little to enhance the model and might de-emphasize the essential mechanics of undulation growth.

#### 4. Coupled equations for the four-layer system

The approach used here consists of decoupling the layers, modeling each layer individually, then finally re-coupling the equations to give a complete description of oxide rumpling. An undulation in the oxide layer gives rise to a sinusoidal normal traction at the interface between the bond coat and oxide and, similarly, at the interface between the oxide and top coat (cf. Fig. 3). These normal tractions deform the creeping layers adjacent to the oxide, causing the undulation to grow if the film is under compression, as it is under most conditions in the present system, or decay if the film is under tension. Provided the bond coat is sufficiently thick compared to the undulation half-wavelength,  $L$ , the stresses resulting from the sinusoidal traction are essentially zero at its lower boundary where it is bonded to the substrate. The same holds for the top coat and its traction-free upper surface. This assertion is valid when the thickness of the layers adjoining the oxide layer satisfies  $h/L \geq 2$  (Balint and Hutchinson, 2003).<sup>3</sup> Under these circumstances the thickness of the bond coat and the top coat can be considered to be infinite for analysis purposes, as will be invoked here, although thickness dependencies can be incorporated.

<sup>3</sup>The growth rate of  $\delta$  is incorrectly plotted as a function of the layer thickness in Fig. 5 of Balint and Hutchinson (2003). The rate becomes smaller as the layer thickness decreases.

An equation for the rate of growth of the undulation that results when a sinusoidal normal traction  $p = p^{(2)} \cos(\pi x_1/L)$  is applied at the top surface of an infinitely thick bond coat with the sense indicated in Fig. 3 was previously derived by Balint and Hutchinson (2003) and is quoted here with temperature dependence of the creep strength incorporated:

$$\dot{\delta}^{(2)} = L \dot{\epsilon}_R^{(2)} e^{-T_R^{(2)}/T} \left( \frac{p^{(2)}}{\sigma_R^{(2)}} \right) \left[ a(n^{(2)}) \left( \frac{\sigma^{(2)}}{\sigma_R^{(2)}} \right)^{n^{(2)}-1} + b(n^{(2)}) \left| \frac{p^{(2)}}{\sigma_R^{(2)}} \right|^{n^{(2)}-1} \right] \tag{9}$$

This result forms the heart of the analytical model. The fact that Eq. (9) accurately captures the nonlinear interaction between the equi-biaxial stress,  $\sigma^{(2)}$ , and the normal traction,  $p^{(2)}$ , is what makes it possible to develop the present model. Based on a finite-element analysis, the elastic strain rates in Eq. (1) were shown to have little direct influence on the undulation growth rate, primarily because the stress distribution for an elastic half-space under the sinusoidal load is not that different from that for the power-law material. Elasticity is neglected in the derivation of Eq. (9) (Balint and Hutchinson, 2003). For a power-law creeping material in the limit  $|p^{(2)}/\sigma^{(2)}| \ll 1$ , the contribution in Eq. (9) from  $a(n^{(2)})$  is the exact solution. In the limit  $\sigma^{(2)} = 0$ , the contribution from  $b(n^{(2)})$  is the exact power-law solution. The highly nonlinear coupling between  $\sigma^{(2)}$  and  $p^{(2)}$  is associated with the contribution from  $a(n^{(2)})$ . Further finite-element work established that the interpolation Eq. (9) is an excellent approximation to  $\dot{\delta}^{(2)}$  over the entire range of  $p^{(2)}/\sigma^{(2)}$ . A perturbation analysis was used to determine the dimensionless coefficient  $a(n^{(2)})$  in the limit  $|p^{(2)}/\sigma^{(2)}| \ll 1$ , and a finite-element computation provided  $b(n^{(2)})$  for the limit  $\sigma^{(2)} = 0$ . An equation similar to Eq. (9) holds for the undulation growth rate of the top coat,  $\dot{\delta}^{(4)}$ . Compatibility requires that the undulation growth rates of the adjoining layers are equal, i.e.  $\dot{\delta}^{(2)} = \dot{\delta}^{(3)} = \dot{\delta}^{(4)}$ .

The oxide film is modeled using von Karman theory for the nonlinear deformation of flat or curved plates or, in this application where there is no  $x_3$ -variation, for a so-called wide beam. The initial undulation at  $t = 0$  is a normal displacement of the centerline of the oxide film:  $w_0(x_1) = \delta_0 \cos(\pi x_1/L)$ . The deflection of the film relative to its initial shape is denoted by  $w(x_1, t)$ , and the deflection of the film measured from the flat state is  $w_{\text{tot}}(x_1, t) = w_0(x_1) + w(x_1, t)$ . As stated earlier, the additional deflection is assumed to maintain the sinusoidal shape of the initial undulation with  $w(x_1, t) = \delta(t) \cos(\pi x_1/L)$  and  $\delta_{\text{tot}}(t) = \delta_0 + \delta(t)$ . Von Karman theory is valid if  $h^{(3)} \ll L$  and the undulation slopes are not more that moderately large, i.e.  $(\partial w_{\text{tot}}/\partial x_1)^2 \ll 1$ , both of which pertain in the present application.

As indicated in Fig. 3, only the normal tractions between the oxide layer and the adjoining layers are taken into account. Creep in the adjoining layers is assumed to relax tangential tractions across the oxide interfaces such that they can be neglected. These assumptions are consistent with the ease of bending the oxide layer compared to the relative difficulty of deforming it in its plane, and they are commonly adopted in modeling film/substrate interactions. Under these circumstances, the average in-plane stress carried by the oxide layer in the von Karman theory,  $\sigma_{11}^{(3)}$ , is independent of  $x_1$ . In the simulations described below,  $\sigma_{11}^{(3)}$  is, with only few exceptions,

compressive such that  $\text{sign}(\sigma_{11}^{(3)}) = -1$ . Under most circumstances, at some point in the isothermal period at 1150 °C the oxide film reaches yield in compression due to the lateral growth; thereafter,  $\sigma^{(3)} = |\sigma_{11}^{(3)}| = \sigma_R^{(3)}$  is maintained until the next cool-down or unloading occurs. While yield occurs, the incremental bending stiffness of the layer is zero and the moment relaxes. Because of the existence of two types of incremental response of the oxide layer, corresponding to elastic ( $\sigma^{(3)} < \sigma_R^{(3)}$ ) and at yield ( $\sigma^{(3)} = \sigma_R^{(3)}$ ), it is useful to partition the additional deflection as

$$w = w_N + \Delta w_e + \Delta w_p. \tag{10}$$

Here,  $w_N$  is the cumulative deflection at the last occurrence of yield or elastic unloading. While the temperature is changing, this corresponds to the end of the  $N$ th thermal cycle under most circumstances. For the current cycle,  $\Delta w_e$  is the incremental deflection relative to the end of the previous cycle, or the point at which unloading began, occurring while the layer responds elastically and  $\Delta w_p$  is the corresponding incremental deflection when the layer is at yield.

With the above notation, the governing equation for the *uncoupled* oxide layer that is valid at all times in the entire thermal history is

$$\begin{aligned} \bar{E}^{(3)} I \frac{\partial^4 \Delta w_e}{\partial x_1^4} - \text{sign}(\sigma_{11}^{(3)}) \sigma^{(3)} h^{(3)} \frac{\partial^2 (w_0 + w_N + \Delta w_e + \Delta w_p)}{\partial x_1^2} \\ = -(p^{(2)} + p^{(4)}) \cos\left(\frac{\pi x_1}{L}\right), \end{aligned} \tag{11}$$

where  $\bar{E}^{(3)} = E^{(3)} / (1 - \nu^{(3)2})$  and  $I = h^{(3)3} / 12$ . As discussed above,  $\Delta w_e$  is zero when the oxide is at yield, and  $\Delta w_p$  is zero when the oxide is not at yield. Once the oxide has yielded and until unloading begins, the bending contribution, the first term in Eq. (11), is absent, modeling the rapid relaxation of the moment that occurs at yield due to the lateral growth strain. This equation applies even when the thickness of the layer increases.

Since all contributions to the deflection in Eq. (10) are assumed to have the sinusoidal shape of the initial deflection such that

$$w = w_N + \Delta w_e + \Delta w_p = (\delta_N + \Delta \delta_e + \Delta \delta_p) \cos(\pi x_1 / L), \tag{12}$$

Eq. (11) admits a separated solution with amplitudes related by

$$Q \Delta \delta_e + P(\delta_0 + \delta_N + \Delta \delta_p) = p^{(2)} + p^{(4)} \tag{13}$$

with

$$\begin{aligned} P &= -\text{sign}(\sigma_{11}^{(3)}) \frac{\sigma^{(3)} h^{(3)} \pi^2}{L^2}, \\ Q &= -\frac{\sigma^{(3)} h^{(3)} \pi^2}{L^2} \left[ \text{sign}(\sigma_{11}^{(3)}) + \left(\frac{L^*}{L}\right)^2 \right], \\ L^* &= h^{(3)} \sqrt{\frac{\pi^2 \bar{E}^{(3)}}{12 \sigma^{(3)}}}. \end{aligned} \tag{14}$$

Following the prescription stated above, in a given cycle,  $\Delta\delta_p = 0$  when the oxide layer is elastic and  $\Delta\delta_e = 0$  while the layer is plastic. At yield,  $\Delta\delta_e$  is added to  $\delta_N$  and then reset to zero. At the end of the isothermal period, or, when unloading begins if that occurs first,  $\Delta\delta_p$  is added to  $\delta_N$  and then it is reset to zero;  $\Delta\delta_e$  is then measured relative to that point.

Growth is completely described by the set of coupled, nonlinear ordinary differential equations presented above. The set cannot be solved analytically, but is readily solved using elementary numerical methods employing Euler time steps. The simulations begin with cool-down at  $t = 0$  starting at the peak temperature,  $T = 1150^\circ\text{C}$ , with an initial undulation,  $\delta_0$ , and initial conditions  $\sigma^{(2)} = \sigma^{(4)} = 0$ ,  $\sigma_{11}^{(3)} = -\sigma_R^{(3)} = -300\text{ MPa}$  and  $h^{(3)} = 0.5\ \mu\text{m}$ . If all quantities are known at time  $t$ , increments for the next time step  $t + dt$  are computed and quantities are updated in the following manner:

- (a) With Eq. (13), the compatibility condition,  $\dot{\delta}^{(2)} = \dot{\delta}^{(4)}$ , and Eq. (9) for the bond coat and top coat,  $p^{(2)}$ ,  $p^{(4)}$  and  $d\delta = \dot{\delta}^{(2)} dt = \dot{\delta}^{(4)} dt$  are computed simultaneously.
- (b)  $d\delta$  is identified with  $d\Delta\delta_e$  or  $d\Delta\delta_p$  depending on whether  $\sigma^{(3)} < \sigma_R^{(3)}$  or  $\sigma^{(3)} = \sigma_R^{(3)}$ , respectively.
- (c)  $d\sigma^{(2)} = \dot{\sigma}^{(2)} dt$ ,  $d\sigma^{(3)} = \dot{\sigma}^{(3)} dt$  and  $d\sigma^{(4)} = \dot{\sigma}^{(4)} dt$  are computed from Eq. (5) for the bond coat and top coat, and Eq. (8).
- (d)  $dh^{(3)} = \dot{h}^{(3)} dt$  and  $d\varepsilon_G = \dot{\varepsilon}_G dt$  are computed from Eqs. (3) and (4).
- (e) If elastic unloading or yielding occurs in the oxide layer in the time step,  $\Delta\delta_e$  or  $\Delta\delta_p$  is reset and  $\delta_N$  is updated.
- (f) All quantities are updated except  $p^{(2)}$  and  $p^{(4)}$  (e.g.  $\Delta\delta_e = \Delta\delta_e + d\Delta\delta_e$ , etc.), then time is advanced to the next step and the process begins again with (a)).

## 5. Simulations of undulation growth for PtNiAl systems without a top coat

In this section, the rumpling that occurs in PtNiAl systems without top coats is simulated in order to elucidate the mechanics and to examine trends relative to experimental measurements, as well as finite-element simulations. For this purpose, the assessment examines five phenomena:

- (1) thermal history effects;
- (2) wavelength and amplitude effects;
- (3) the role of the martensite transformation;
- (4) TGO thickness effects;
- (5) the influence of heating/cooling rate.

### 5.1. Thermal history effects

The observation that far more undulation growth occurs in PtNiAl systems subject to cyclic thermal histories than for isothermal histories for the same total

time at 1150 °C, or hot time, has been explored by analytic and finite-element models (Karlsson and Evans, 2001; Karlsson et al., 2002; Xu et al., 2003), as well as in an earlier version of the present model (Balint and Hutchinson, 2003). A set of simulations, shown in Fig. 6, illustrates the difference between cyclic and isothermal histories. Amplitude growth is normalized by the initial oxide thickness. Undulation growth, with or without the top coat, is promoted by the equi-biaxial stress in the bond coat. During heat-up and hold at 1150 °C while the equi-biaxial stress is relaxing, the bond coat is susceptible to undulation growth arising from the normal pressure exerted on it by the oxide layer. It is the presence of the first term in Eq. (9) with the coefficient  $a(n^{(2)})$  that accounts for the nonlinear interaction between the equi-biaxial stress and the normal pressure; the contribution of the second term in Eq. (9) is small by comparison, especially in the absence of the top coat, since the values of the normal stress are much lower than the equi-biaxial stress when the creep strength of the bond coat is low. The equi-biaxial stress in the bond coat relaxes rapidly by creep at elevated temperatures, and, once it is zero, it remains so for the remainder of the isothermal period effectively shutting down further undulation growth during that cycle, apart from the contribution of the second term in Eq. (9). A cyclic history renews the stress in the bond coat each time the temperature is raised to 1150 °C, thereby producing an increment of growth each

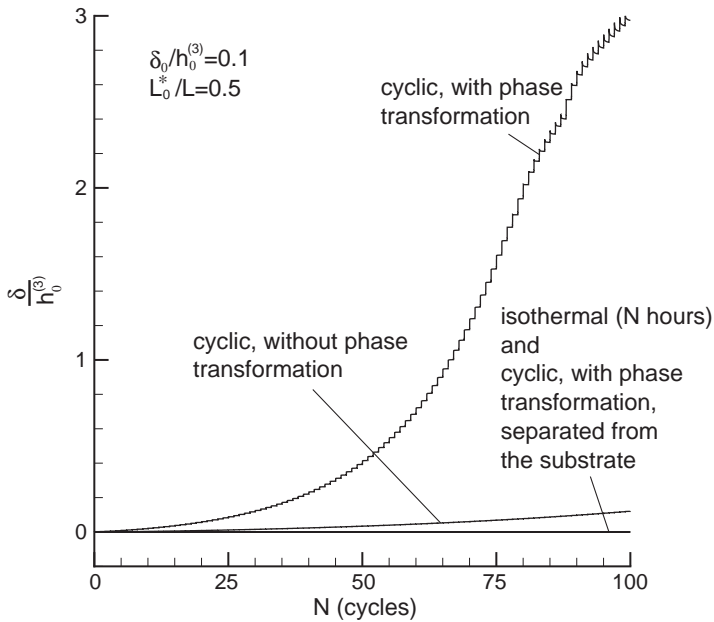


Fig. 6. Shown here: (1) no undulation growth occurs on oxidized bulk PtNiAl (i.e. a thick layer of PtNiAl separated from the substrate); (2) the phase transformation leads to much more undulation growth ( $\delta_{N=100} = 1.5 \mu\text{m}$  with the transformation,  $\delta_{N=100} = 0.06 \mu\text{m}$  without it); and (3) appreciable undulation growth does not occur under isothermal conditions for the initial undulation sizes used here.

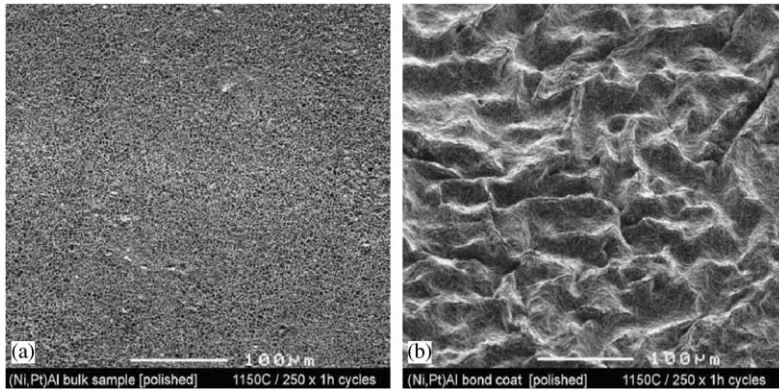


Fig. 7. Specimens tested by Tolpygo and Clarke (2003) showing: (a) a thermally cycled, unconstrained bulk PtNiAl bond coat and (b) a PtNiAl bond coat attached to a thick substrate that is subjected to an identical cyclic thermal history. The constraining effect of the substrate prevents the PtNiAl bond coat from expanding or contracting freely as the temperature changes, which leads to a large equi-biaxial stress. This greatly reduces its creep strength, which enables undulation growth to occur.

cycle. The lateral expansion and compaction of the substrate is necessary to produce the equi-biaxial stress in the bond coat as demonstrated by the experiments of Tolpygo and Clarke (2003) shown in Fig. 7. Model simulations in Fig. 6 predict very little rumpling on a bulk PtNiAl bond coat unsupported by a substrate.

Most of the undulation growth that occurs in a given thermal cycle occurs during heat up at temperatures above 600 °C and in the early portion of the hold period at 1150 °C. As described earlier, once the in-plane stresses in the bond coat have relaxed, most undulation growth ceases. There is a distinction between systems with and without a top coat in this respect. A significantly larger fraction of undulation growth is found to take place during the time at the peak temperature for systems with a top coat.

### 5.2. Wavelength and amplitude effects

Complete, 100-cycle simulations shown in Fig. 8 reveal the preference for certain wavelengths (recall that the oxide layer thickens while at 1150 °C, increasing from 0.5 μm at  $t = 0$  to 3 μm at  $N = 100$ ). At any stage of the cyclic history, the wavelength with the largest growth rate scales with  $L^* = h^{(3)} \sqrt{\pi^2 \bar{E}^{(3)} / 12\sigma^{(3)}}$ , which increases as the TGO thickens. This length is the half-wavelength of a sinusoidal buckling mode for a periodically pinned oxide layer of thickness  $h^{(3)}$  subject to compressive stress  $\sigma^{(3)}$  corresponding to the onset of buckling. It reflects a balance between the elastic bending stiffness and the compressive stress in the oxide layer. If the oxide layer were to remain elastic, bending effects would overcome the compressive stress to reduce undulations for  $L < L^*$ , and vice versa for  $L > L^*$ . To present results in dimensionless form, we define a reference length associated with the

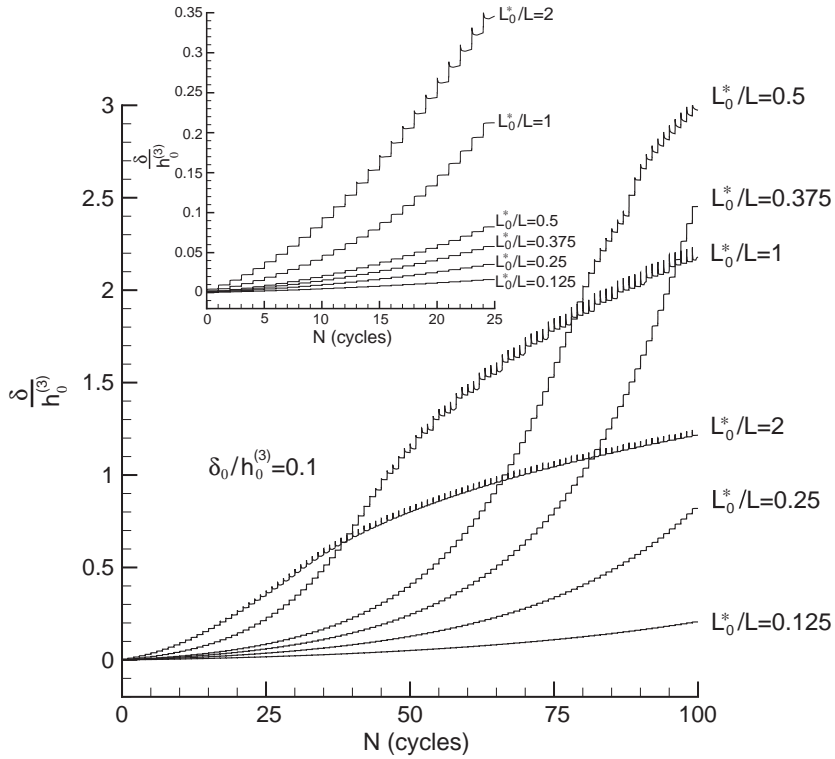


Fig. 8. Complete, 100-cycle simulations for PtNiAl systems without a top coat. The inset shows that undulations that grow the quickest early in the thermal history have shorter wavelengths than those that give the greatest total growth over 100 cycles.

initial oxide thickness,  $h_0^{(3)}$  ( $0.5 \mu\text{m}$  in the simulations):

$$L_0^* = h_0^{(3)} \sqrt{\frac{\pi^2 \bar{E}^{(3)}}{12 \sigma_R^{(3)}}} \tag{15}$$

with  $\sigma_R^{(3)}$  as the yield stress at  $1150 \text{ }^\circ\text{C}$ . Even though the oxide layer yields during the high temperature hold period, the reference length (15) retains its role as the primary scale factor for the critical undulation wavelength.<sup>4</sup>

When the number of cycles is less than roughly 25 the undulations with the shorter wavelengths grow the most rapidly, reflecting the fact that the TGO is still relatively thin. However, as the number of cycles increases and the oxide layer thickens, longer wavelength undulations grow at faster rates, overtaking the shorter wavelengths.

<sup>4</sup>An alternative definition of the reference length in Eq. (15) could use the thickness of the oxide layer at, for example, 100 h at peak temperature. The choice based on the initial TGO thickness,  $h_0^{(3)}$ , is somewhat arbitrary, but changing to another choice of layer thickness simply involves a multiplicative change in  $L_0^*$ .

The undulation that is growing the fastest at 100 cycles has  $L_0^*/L \cong 0.375$  but the undulation that has the largest *amplitude* at 100 cycles has  $L_0^*/L \cong 0.5$ . The model shows that  $L^*/L$  is approximately constant for the undulations growing the fastest at any point in the cyclic thermal history. Equivalently, the wavelength,  $L$ , of the fastest growing undulation increases in proportion to the TGO thickness  $h^{(3)}$  as it increases. Undulation growth rates are quite sensitive to the values of the property parameters used in the simulations, especially the high temperature creep strength of the bond coat, the lateral growth strain per cycle and high temperature yield stress of the oxide layer.

We note in passing that some undulation growth is possible even when there is no thermal expansion mismatch between a bond coat and its substrate. Simulations under such circumstances reveal that the second term in Eq. (9), which is nonlinear in the normal pressure between the undulation and bond coat, then becomes dominant. (This term is relatively unimportant when the expansion mismatch is significant.) However, for appreciable undulation growth to occur, initial undulations must be considerably larger than those invoked in the simulations of Fig. 6. A higher yield stress of the oxide layer at the peak temperature also promotes undulation growth in systems without appreciable thermal mismatch (Karlsson and Evans, 2001; Xu et al., 2003).

One source of initial undulations identified by Tolpygo and Clarke (2004b) is the grain pattern of the bond coat on which the oxide layer grows. Once a wavelength of the undulation emerges, it tends to persist. In PtNiAl systems, it has been observed that the troughs of the oxide layer tend to coincide with the bond coat grain boundaries, and these troughs are amplified by thermal cycling. The formation of the troughs is thought to be due to differential swelling of grains in the interior of the bond coat and along its boundary (Tolpygo and Clarke, 2004b), an effect that is not incorporated in the present model. However, the present model can be adapted to accommodate initial undulations of this type, and it has been able to successfully reproduce features tied to the grains.

### 5.3. Martensite transformation

Fig. 6 also illustrates the importance of the phase transformation. The undulation amplitude grows by  $1.5 \mu\text{m}$  in 100 cycles for an undulation with initial amplitude of  $0.05 \mu\text{m}$ , but only grows by  $0.06 \mu\text{m}$  when the phase transformation is suppressed. The effect can be interpreted in terms of a significantly higher thermal expansion mismatch within the transformation range. The impact of the phase transformation is explored further in Fig. 9. The four temperatures at points 2, 3, 6 and 7 in Fig. 5 that characterize the hysteresis loop have been shifted in increments of  $100^\circ\text{C}$  for the simulations of Fig. 9 (i.e. the loop in Fig. 5 remains unchanged apart from an overall temperature shift). Plotted in Fig. 9 is the total undulation growth after 100 cycles against the inverse of the normalized half-wavelength of the undulation. At a given wavelength, it is clear that shifting the phase transformation, even if only slightly, can have a dramatic effect on undulation growth. Shifting the hysteresis loop by  $-100^\circ\text{C}$  reduces  $(\delta/h_0^{(3)})_{N=100}$  by as much as 60%, and a shift of  $-200^\circ\text{C}$  provides a

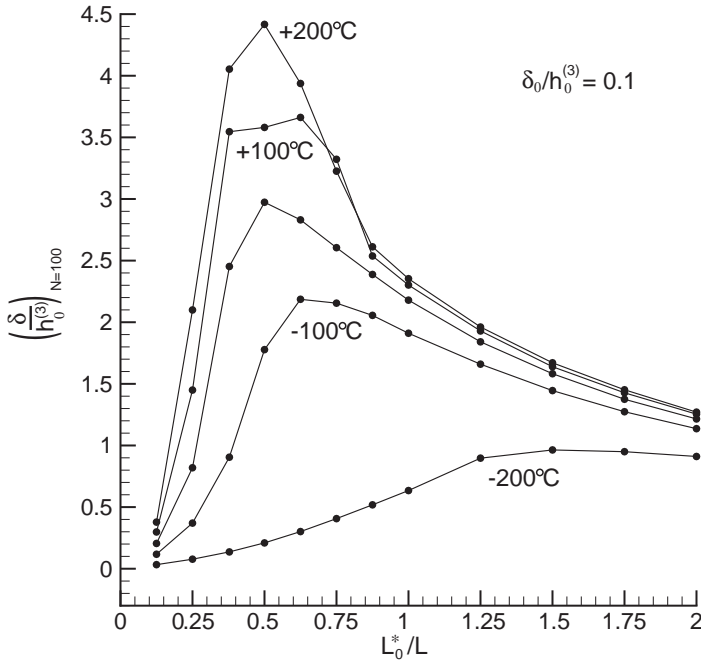


Fig. 9. Total undulation growth after 100 cycles plotted against the inverse of the normalized half-wavelength. The four temperatures at points 2, 3, 6 and 7 in Fig. 5 that characterize the hysteresis loop of the phase transformation have been shifted together in increments of 100 °C. Rumpling can be reduced significantly by shifting the hysteresis to lower temperatures.

reduction over 90%. As discussed in connection with Fig. 4, the shift reduces the stress in the bond coat during that part of a thermal cycle when it is most susceptible to transverse deformation ( $T > 600$  °C), i.e. when the creep strength is low. Shifting the phase transformation to lower temperatures is a potentially viable way of reducing rumpling.

#### 5.4. TGO thickness effects

More rumpling has been observed on systems with thick oxide layers than on those with thin layers, all other factors being equal, as shown in Fig. 10 for specimens tested by Tolpygo and Clarke (2003). The oxide layer was formed by isothermal exposure to high temperature producing relatively small initial undulations. The systems were then cycled. The model also predicts more rumpling for the thicker oxide layers. The upper curve in Fig. 11 is the total undulation amplitude after 100 cycles, normalized by the amplitude at  $t = 0$ , computed for an oxide layer whose thickness is maintained at 10  $\mu\text{m}$ , while the lower curve has been computed for a constant thickness layer of 5  $\mu\text{m}$ . The initial undulation amplitude is the same for both cases,  $\delta_0 = 0.05$   $\mu\text{m}$ , as is the lateral growth strain per cycle, whose

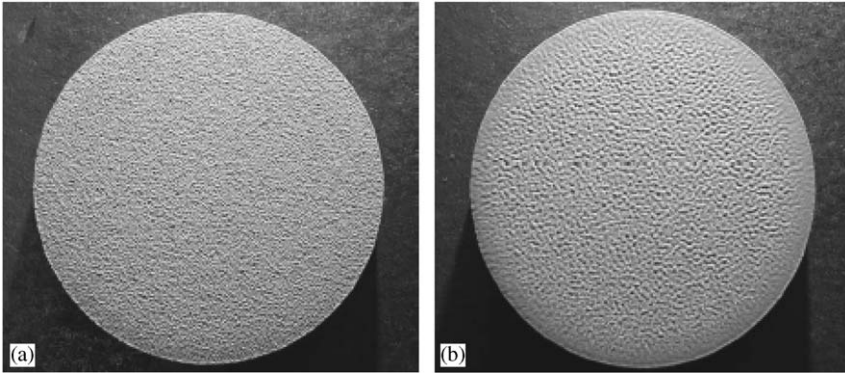


Fig. 10. PtNiAl specimens tested by Tolpygo and Clarke (2003) showing the effect of oxide thickness on rumpling. The oxide thickness is roughly 5  $\mu\text{m}$  in (a) and 10  $\mu\text{m}$  in (b). The systems were subjected to the same cyclic thermal history with a total of 200 h at the peak temperature. Considerably more rumpling occurs for the specimen with the thicker oxide layer.

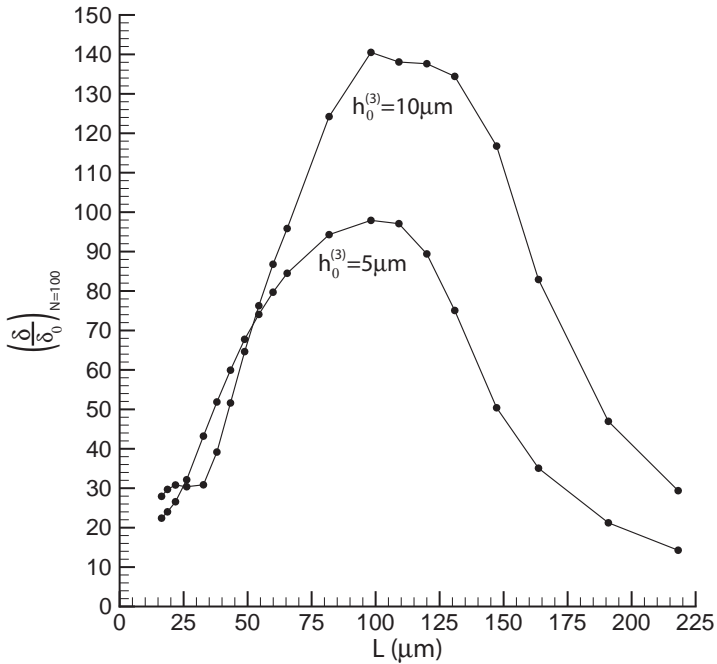


Fig. 11. Total undulation growth after 100 cycles plotted against half-wavelength. The oxide thickness is held constant at 5  $\mu\text{m}$  for the lower curve and 10  $\mu\text{m}$  for the upper curve, and the lateral growth strain is incremented linearly to 5% over 100 h at 1150  $^{\circ}\text{C}$ . In both cases, the initial undulation amplitude is  $\delta_0 = 0.05 \mu\text{m}$ . Thicker oxide layers experience more undulation growth (cf. Fig. 10).

rate is constant and gives a total of 5% in 100 cycles. The incremental bending stiffness of the thicker oxide layer is greater which inhibits rumpling. However, the compressive force per unit length in the thicker oxide is also greater which counteracts the larger bending stiffness and encourages rumpling.

### 5.5. Heating/cooling rate effects

The fact that a significant fraction of undulation growth for the system without the top coat occurs during heat-up suggests that the amount of rumpling might depend on the duration of the heat-up. The effect is shown in Fig. 12 where the total undulation amplitude after 100 cycles is plotted against the inverse of the normalized half-wavelength for various heat-up times,  $t_{hc}$ . The duration of cool-down is taken to be the same as heat-up, and the duration of the high-temperature hold is 1 h for all cases. Less rumpling occurs for a shorter heat-up because there is less time for the undulation to grow while the bond coat is most susceptible to transverse deformations. However, there is also less time for the stress in the bond coat to decay. A larger stress in the bond coat at the beginning of the hold at 1150 °C is mitigated by the fact that the magnitude of the stress in the oxide, the driving force for undulation growth, is less at the beginning of the 1150 °C hold period than during

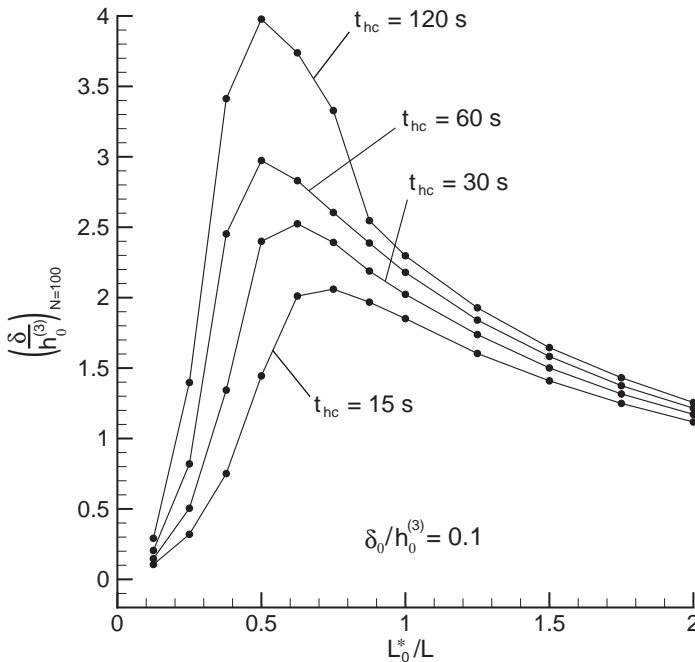


Fig. 12. Total undulation growth after 100 cycles plotted against the inverse of the normalized half-wavelength. The duration of the heat-up has been varied between 15 s and 2 min and the total time at 1150 °C is 100 h for all simulations. Less rumpling occurs for thermal histories with shorter heat-up times.

any other part of a thermal cycle. Thus, the overall potential for undulation growth is diminished by decreasing the duration of the heat-up. The effect is most pronounced near the critical wavelength. A decrease of the heat-up time by roughly a factor of ten produces about a 75% decrease in the undulation amplitude at the conclusion of thermal cycling. It should be noted that the effect illustrated by Fig. 12 would be suppressed if a top coat were included in the simulations because the top coat significantly reduces undulation growth during heat-up, as discussed in the next section.

**6. Simulations of undulation growth for PtNiAl systems with a top coat**

Even without a ceramic top coat a TBC system has a large set of parameters that influence rumpling rates, and the results in the previous section only enumerate a few of the many trends of potential interest. A top coat introduces even more parameters and further complicates the mechanics of undulation growth. To illustrate the role of the top coat, the study presented in Fig. 8 is repeated in Fig. 13 for precisely the same

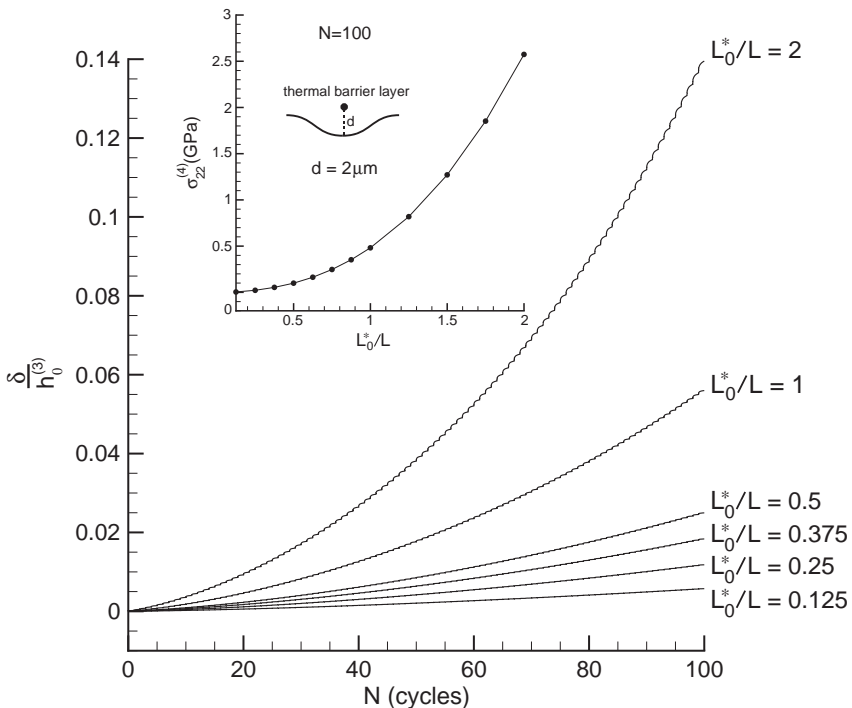


Fig. 13. Complete, 100-cycle simulations for PtNiAl systems with a top coat. The inset shows the tensile stress,  $\sigma_{22}^{(4)}$ , at room temperature after 100 cycles,  $2 \mu\text{m}$  above the valley of an undulation, plotted against the inverse of the normalized half-wavelength.

system, but with a top coat included. The undulation wavelengths considered are assumed to be sufficiently short that the top coat, like the bond coat, can be taken to be infinitely thick. Creep data for YSZ at temperatures as high as 1150 °C is not available, although indentation tests have revealed that the top coat material creeps readily at high temperatures. In the absence of adequate data, the top coat is assumed to be roughly 10 times more creep-resistant than the bond coat. Specifically, the strain rates in the top coat are given by an equation of the same form as Eq. (1) with  $\sigma_R^{(4)} = 4\sigma_R^{(2)} = 100$  MPa and  $\dot{\epsilon}_R^{(4)} = 25\dot{\epsilon}_R^{(2)} = 5$  s<sup>-1</sup>, but with the same temperature variation,  $T_R^{(4)} = 15 \times 10^3$  K, and power-law exponent,  $n^{(4)} = 4$ . The stress in the top coat is governed by an equation of the same form as Eq. (5) with due regard for the material parameters. The thermal expansion coefficient for the top coat is  $\alpha^{(4)} = 10 \times 10^{-6}$  °C<sup>-1</sup>. Contrary to the case without a top coat, no critical wavelength exists, for a system that is cycled 100 times, within the set of wavelengths deemed representative of initial imperfections in a real thermal barrier system. Rather, the shortest wavelength gives the greatest total undulation growth. Even though the top coat creeps readily, it significantly restrains undulation growth. For the creep parameters assumed here, more than a ten-fold reduction in the maximum total undulation growth occurs when the top coat is included. Nevertheless,  $\delta/h_0^{(3)} = 0.14$  (cf. Fig. 13) can lead to very large stresses in the top coat. The tensile stress in the top coat above the valley of an undulation (which can lead to crack formation parallel to the interface) is relatively small at high temperatures when the top coat is soft, but can be large at room temperature when the top coat is elastic. A good estimate of this stress, at room temperature, follows from the solution for an elastic half-space with a sinusoidal normal pressure applied at its free surface. The inset in Fig. 13 shows the stress  $\sigma_{22}^{(4)}$  calculated in this manner at 25 °C, 2  $\mu$ m above the valley of an undulation. The stresses correspond to the  $\delta$  values at  $N = 100$  for each simulation depicted in the main figure. Stresses as large as 3 GPa are possible for the wavelengths considered, which are in the range needed to begin the process of crack formation and coalescence that ultimately leads to spallation of the top coat.

## 7. Concluding remarks

A comprehensive analytical model of TGO rumpling that occurs as the temperature is cycled in a four-layer thermal barrier system has been presented. Undulation growth is driven by the lateral growth strain in the TGO and occurs at a rate governed by many factors, including power-law creep of the bond coat and plastic yielding of the TGO. Consistent with prior assessments (Karlsson and Evans, 2001; Karlsson et al., 2002; Xu et al., 2003), it can be concluded from the results presented in this paper that increasing the bond coat creep strength or reducing the high temperature strength of the TGO reduce undulation growth, although the advantage of the latter is mitigated by the more ready loss of the elastic bending stiffness of the TGO that accompanies a decrease of its strength. The present model is also consistent with previous work in that reducing the initial undulation

amplitude reduces undulation growth (Karlsson and Evans, 2001). A number of other important experimental observations made on PtNiAl bond coat systems without top coats have been reproduced.

Details of rumpling as predicted by the model depend on the bond coat material. In all cases, rumpling driven by a compressed, undulating oxide film is governed by the highly nonlinear power-law creep behavior of the bond coat. For PtNiAl systems, the combination of thermal expansion mismatch and the martensite transformation produces a relatively large equi-biaxial stress in the bond coat at high temperatures. Until this stress is relaxed, the bond coat is especially susceptible to undulation growth. Thus, there is a period of susceptibility in each thermal cycle, primarily during the last stages of heat-up. This accounts for the significant difference in undulation growth for this system between cyclic and isothermal histories, as well as the observed trend for total undulation growth with hot time per cycle. For the first time, it has been shown that modifying the martensite transformation in the bond coat by shifting the hysteresis to lower temperatures, which decreases the equi-biaxial stress in the bond coat at elevated temperatures, can dramatically reduce rumpling; a shift of  $-200\text{ }^{\circ}\text{C}$  reduces total undulation growth by a factor of ten. Shifting the transformation temperatures by minor compositional changes, if feasible, is a potentially viable strategy to modify the design of PtNiAl thermal barrier coatings for longer lifetimes.

Although high-temperature creep parameters are currently unavailable for YSZ, calculations show that a top coat that is roughly ten times more creep-resistant than PtNiAl also reduces undulation growth by a factor of ten or more compared to a system without a top coat. This level of undulation growth is still sufficient to give rise to tensile stresses at room temperature on the order of several GPa above undulation valleys.

The present analytical model, in its most complete form, should serve as a tool to guide future design of thermal barrier coatings. As mentioned in the Introduction, the number of parameters characterizing the materials, geometry and thermal histories of a TBC is large. Finite-element modeling of specific aspects of TBC behavior will be required to provide more refined results than the present model can provide. However, a TBC subject to hundreds of thermal cycles is a computationally intensive problem making extensive parameter studies such as those presented here prohibitively difficult. The present model can very rapidly generate trends and identify the most important parameters affecting rumpling, thereby significantly narrowing the required number of more refined finite-element simulations.

## **Acknowledgements**

This work was supported in part by the ONR MURI grant entitled “Prime Reliant Coatings” and in part by the Division of Engineering and Applied Sciences at Harvard University. The authors are indebted to A.G. Evans for many helpful suggestions.

## References

- Balint, D.S., Hutchinson, J.W., 2003. Undulation instability of a compressed elastic film on a nonlinear creeping substrate. *Acta Mater.* 51, 3965–3983.
- Chen, X., Hutchinson, J.W., He, M.Y., Evans, A.G., 2003a. On the propagation and coalescence of delamination cracks in compressed coatings: with application to thermal barrier systems. *Acta Mater.* 51, 2017–2030.
- Chen, M.W., Ott, R.T., Hufnagel, T.C., Wright, P.K., Hemker, K.J., 2003b. Microstructural evolution of platinum modified nickel aluminide bond coat during thermal cycling. *Surf. Coat. Technol.* 163–164, 25–30.
- Clarke, D.R., 2003. The lateral growth strain accompanying the formation of a thermally grown oxide. *Acta Mater.* 51, 1393–1407.
- Evans, A.G., He, M.Y., Hutchinson, J.W., 2001a. *Prog. Mater. Sci.* 46, 249–271.
- Evans, A.G., Mumm, D.R., Hutchinson, J.W., Meier, G.H., Pettit, F.S., 2001b. *Prog. Mater. Sci.* 46, 505–553.
- Karlsson, A.M., Evans, A.G., 2001. A numerical model for the cyclic instability of thermally grown oxides in thermal barrier systems. *Acta Mater.* 49, 1793–1804.
- Karlsson, A.M., Hutchinson, J.W., Evans, A.G., 2002. A fundamental model of cyclic instabilities in thermal barrier systems. *J. Mech. Phys. Solids* 50, 1565–1589.
- Mumm, D.R., Evans, A.G., Spitsberg, I.T., 2001. Characterization of a cyclic displacement instability for a thermally grown oxide in a thermal barrier system. *Acta Mater.* 49, 2329–2340.
- Pan, D., Chen, M.W., Wright, P.K., Hemker, K.J., 2003. Evolution of a diffusion aluminide bond coat for thermal barrier coatings during thermal cycling. *Acta Mater.* 51, 2205–2217.
- Tolpygo, V.K., Clarke, D.R., 2000. Surface rumpling of a (Ni, Pt)Al bond coat induced by cyclic oxidation. *Acta Mater.* 48, 3283–3293.
- Tolpygo, V.K., Clarke, D.R., 2003, unpublished research.
- Tolpygo, V.K., Clarke, D.R., 2004a. On the rumpling mechanism in nickel-aluminide coatings. Part I: an experimental assessment. *Acta Mater.* 52, 5115–5127.
- Tolpygo, V.K., Clarke, D.R., 2004b. On the rumpling mechanism in nickel-aluminide coatings. Part II: characterization of surface undulations and bond coat swelling. *Acta Mater.* 52, 5129–5141.
- Xu, T., He, M.Y., Evans, A.G., 2003. A numerical assessment of the durability of thermal barrier systems that fail by ratcheting of the thermally grown oxide. *Acta Mater.* 51, 3807–3820.